Water Resources Research

RESEARCH ARTICLE
10.1029/2021WR031194

Modeling the Organic Carbon Oxidation and Redox Sequence Under the Partial-Equilibrium Approach: A Discussion by Means of a Semi-Analytical Solution

Maarten W. Saaltink[1,2] and Paula Rodríguez-Escales[1,2]

[1]Department of Civil and Environmental Engineering, Universitat Politècnica de Catalunya (UPC), Barcelona, Spain, [2]Associated Unit: Hydrogeology Group (UPC-CSIC), Barcelona, Spain

Key Points:

- A semi-analytical solution for organic carbon oxidation has been developed
- The partial equilibrium approach combined with diffusion can give spurious oxidation reactions
- The fully kinetic and partial equilibrium approach give similar results for advective cases

Correspondence to:
M. W. Saaltink,
maarten.saaltink@upc.edu

Citation:
Saaltink, M. W., & Rodríguez-Escales, P. (2022). Modeling the organic carbon oxidation and redox sequence under the partial-equilibrium approach: A discussion by means of a semi-analytical solution. *Water Resources Research*, *58*, e2021WR031194. https://doi.org/10.1029/2021WR031194

Received 8 SEP 2021
Accepted 29 MAY 2022

Abstract In this work, we have developed a semi-analytical solution for organic carbon oxidation coupled to the reduction-oxidation sequence assuming the Partial Equilibrium Approach (PEA) and using the decoupling procedure of De Simoni et al. (2005), https://doi.org/10.1029/2005WR004056. Our solution was applied to two very simple cases. The first assumes only advective transport and the second only diffusive transport. Comparison with a numerical solution showed the adequacy of our analytical solution to be implemented in several scenarios, for example, in organic carbon oxidation in the unsaturated zone or in highly heterogeneous advective domains. We found that for the diffusion case the PEA produced spurious reactions, such as oxidation of N_2 by O_2 when compared with an approach using full kinetics. These reactions do not occur in the advection case. An analysis with the semi-analytical solution revealed that they are the result of a combination of diffusive fluxes and the fact that the PEA assumes the electron acceptors to react with each other in equilibrium. Our analytical solutions are capable to quantify this shortcoming, becoming a tool to validate numerical models using PEA to describe organic carbon oxidation.

1. Introduction

The fate of organic carbon is a key aspect to understand the geochemistry of an aquifer. The organic matter, by means of its organic carbon and nitrogen, acts as electron donor oxidizing the terminal electron acceptors (TEAs) present in the hydrochemistry system and defining the reduction-oxidation (redox) potential. Consequently, water loses its oxidants in a sequence that follows the redox potential, Eh (or pe), from more positive (or high) to more negative (or low) values in coherence with the Gibb's free energy of the half reactions. Most of the redox reactions in subsurface occurs thanks to microbial catalysis, which mediates the electron transfer to obtain a source energy to synthesize new cells and to maintain the old ones already formed.

Typically, during organic carbon oxidation the water chemistry may change by reducing the TEAs concentration (typically in this order O_2, NO_3^-, Mn^{4+}, Fe^{3+}, SO_4^{2-}) or through the appearance of the reaction products (e.g., N_2, Mn^{2+}, Fe^{2+}, H_2S, CH_4). Thus, redox geochemistry implies a set of complex and heterogeneous reactions involving gases, ionic species and iron, manganese and sulfate minerals (Christensen et al., 2000). Consequently, it plays an important role in the water quality of different environmental systems like marine (Jaffé et al., 2008; Middelburg, 1989) or lake sediments (Canavan et al., 2007; Torres et al., 2015), polluted systems such as landfill leachate pollution (Brun & Engesgaard, 2002; Brun et al., 2002; Rolle et al., 2008; van Breukelen et al., 2004) or in wetlands (Dash et al., 2020; Lee et al., 2019; Ng et al., 2017, 2020) and managed aquifer recharge applications (Barba et al., 2019; Rodríguez-Escales et al., 2020; Valhondo et al., 2015).

Numerical modeling of redox systems has been extensively documented in the literature. These models consider the complexity of the redox geochemistry by coupling the oxidation of organic carbon with the sequential reduction of the TEAs, plus the role of microorganisms as catalyzers and as sink of organic carbon. Because of microbial catalysis, it is widely accepted that reduction–oxidation systems are far away from thermodynamic equilibrium (Stumm & Morgan, 1996) and oxidation of organic carbon is usually represented kinetically. In literature, organic carbon oxidation and the subsequent redox zonation are modeled following two main strategies.

The first one is based on fully kinetic reduction of TEAs. Typically, the rate laws used to predict microbial respiration (and consequently TEAs concentration) are Monod and dual-Monod equations (e.g., Arora et al., 2015; Jin & Bethke, 2003; Mayer et al., 2001; Schäfer et al., 1998a, 1998b; Van Cappellen and Gaillard, 1996). The

redox sequence is modeled by an inhibition switch in the Monod equation [$k_i / (k_i + c_i)$, where k_i is the inhibition parameter and c_i is the concentration of the TEA]. Then, the presence of TEAs with a higher reduction potential inhibits reactions with lower ones. This approach is realistic in some situations. For example, O_2 can inactivate some enzyme systems of methanogenic bacteria (Curtis, 2003), which is well represented by an inhibition term. Nevertheless, the use of inhibition terms is not accurate in anoxic systems since the free energies of H_2 with TEAs such as Fe^{3+} oxides, SO_4^{2-}, and CO_2 may be indistinguishable within the experimental error (Postma & Jakobsen, 1996). Consequently, some TEAs are used concomitantly. For example, Cozzarelli et al. (2000) observed concomitant sulfate reduction and methanogenesis in the anoxic portion of a landfill leachate. Others also observed concomitant sulfate and iron reduction (Hansel et al., 2015; Postma & Jakobsen, 1996). Consequently, the use of Monod kinetics can produce unrealistic redox zonation and pH simulations (Curtis, 2003; Jin & Bethke, 2003).

The second strategy assumes local equilibrium of the TEAs. This Partial Equilibrium Approach (PEA) was first defined by Postma and Jakobsen (1996). It decouples the redox systems in two half reactions. The oxidation of organic carbon is assumed to be the rate-determining step and is controlled by a defined kinetic rate law (e.g., first order, Monod, or dual Monod). On the other hand, the reduction of TEAs is assumed to be fast and by equilibrium, that is, according to equilibrium reactions and Gibbs free energy. Contrarily to the fully kinetic strategy, which is disconnected from thermodynamics, the use of the PEA guarantees that TEAs will be reduced only when there exists a favorable Gibbs free energy in the solution. The PEA has been used in several models (Greskowiak et al., 2006; Jakobsen, 2007; Ng et al., 2020; Rodríguez-Escales et al., 2020; van Breukelen et al., 2004). However, one should be careful about the equilibrium conditions. Especially in the field, nonequilibrium conditions may be caused by many factors such as slow kinetics, slow mass transfer, fast water velocities or the co-occurrence of mineral oxides with different thermodynamic stabilities (Curtis, 2003).

In addition to numerical models, analytical and semi-analytical models have been developed as well. In general, (semi-)analytical solutions require more simplified assumptions on geometry and physical/chemical processes, but their calculation is fast and they do not suffer from numerical errors. Because of the last, they are often used to verify numerical model codes. Perhaps more importantly, though often disregarded, they can give a better understanding of the modeled phenomena. An example is the work of De Simoni et al. (2005), who developed a procedure to solve reactive transport for cases with a general set of equilibrium aqueous complexation and precipitation-dissolution reactions. From this the authors concluded that reaction rates are driven by mixing processes. This procedure has been applied to derive analytical and semi-analytical solutions for calcite dissolution in coastal environments (De Simoni et al., 2007; Guadagnini et al., 2009; Romanov & Dreybrodt, 2006). Moreover, it has been extended to include kinetic reactions (Sanchez-Vila et al., 2010) and to incorporate chemical reactions into multiphase flow models for CO_2 storage (Saaltink et al., 2013). With respect to organic carbon oxidation, traditional analytical solutions (e.g., van Genuchten & Alves, 1982) only contemplate one reduction step following a linear kinetic rate law. Others (Chu et al., 2005; Cirpka & Valocchi, 2007) also focus on the effect of transverse dispersion and incomplete mixing. Furthermore, these analytical solutions are constructed using kinetic expressions without considering the thermodynamic limitations and omit the reduction-oxidation sequence.

Considering all of these, the main objective of this work is to develop a semi-analytical solution for organic carbon degradation based on the PEA and the procedure of De Simoni et al. (2005). To do so, we first give some theoretical background on the fully kinetic approach and PEA (Section 2). Then, in Section 3, we present our semi-analytical solution. Section 4 illustrates the solution by two simple examples. This section also contains a verification with a geochemical code (Phreeqc) and, as a secondary objective, an analysis of the differences between the fully kinetics and PEA, using our semi-analytical solution. The last two sections are devoted to the discussions and conclusions.

2. Theoretical Background

2.1. Organic Carbon Oxidation Through Fully Kinetic Models

The organic carbon (expressed as CH_2O) can be oxidized sequentially by various TEAs, for instance:

$$CH_2O + O_2 \rightarrow HCO_3^- + H^+$$

$$CH_2O + 0.8NO_3^- \rightarrow HCO_3^- + 0.4N_2 + 0.4H_2O + 0.2H^+$$

$$CH_2O + 4Fe(OH)_3 + 7H^+ \rightarrow HCO_3^- + 4Fe^{2+} + 10H_2O$$

$$CH_2O + 0.5H_2O \rightarrow 0.5HCO_3^- + 0.5CH_4 + 0.5H^+$$

Kinetic rate laws for the oxidation of organic carbon by the above reactions have to be formulated. A widespread tactic is to use Monod rate laws that inhibit the oxidation by a given TEA if previous TEAs in the oxidation sequence are present. For the above reactions this gives (Van Cappellen & Gaillard, 1996):

$$r_O = \lambda_O(CH_2O)\frac{(O_2)}{k_{O_2} + (O_2)} \quad (1)$$

$$r_N = \lambda_N(CH_2O)\frac{\left(NO_3^-\right)}{k_{NO_3^-} + \left(NO_3^-\right)}\frac{k_{i,O_2}}{k_{i,O_2} + (O_2)} \quad (2)$$

$$r_{Fe} = \lambda_{Fe}(CH_2O)\frac{(FeIII)}{k_{FeIII} + (FeIII)}\frac{k_{i,NO_3^-}}{k_{NO_3^-} + \left(NO_3^-\right)}\frac{k_{i,O_2}}{k_{i,O_2} + (O_2)} \quad (3)$$

$$r_C = \lambda_C(CH_2O)\frac{(DIC)}{k_{DIC} + (DIC)}\frac{k_{i,FeIII}}{k_{i,FeIII} + (FeIII)}\frac{k_{i,NO_3^-}}{k_{i,NO_3^-} + \left(NO_3^-\right)}\frac{k_{i,O_2}}{k_{i,O_2} + (O_2)} \quad (4)$$

where λ_x are kinetic rate law parameters [time^{-1}] for the different TEAs (x); k_x and $k_{i,x}$ are half-saturation and inhibition constants, respectively; ( ) refers to concentrations, and DIC is dissolved inorganic carbon. As a first approximation, the half-saturation and inhibition constants can be assumed equal ($k_x = k_{i,x}$) (Van Cappellen and Gaillard, 1996). If, in addition, the λ_x parameters of all reactions are the same ($\lambda_O = \lambda_N = \lambda_{Fe} = \lambda_C = \lambda$), the total oxidation rate of organic carbon ($r_k = r_O + r_N + r_{Fe} + r_C$) is:

$$r_k = \lambda\,(CH_2O)\left(\frac{(O_2)}{k_{O2} + (O_2)} + \frac{k_{O2}}{k_{O2} + (O_2)}\left(\frac{\left(NO_3^-\right)}{k_{NO3} + \left(NO_3^-\right)} + \frac{k_{NO3}}{k_{NO3} + \left(NO_3^-\right)}\left(\frac{(FeIII)}{k_{FeIII} + (FeIII)} + \frac{k_{FeIII}}{k_{FeIII} + (FeIII)}\frac{(DIC)}{k_{DIC} + (DIC)}\right)\right)\right) \quad (5)$$

The second assumption ($\lambda_O = \lambda_N = \lambda_{Fe} = \lambda_C = \lambda$) makes sense if the different reduction rates are similar. Various authors have followed similar λ_x (e.g., Hunter et al., 1998; Ng et al., 2017) and other authors have fitted similar values (in the same order of magnitude) in models considering different TEAs (Rolle et al., 2008). If one or more of the TEAs has a concentration much higher than its half-saturation (i.e., $(x) \gg k_x \Rightarrow (x)/(k_x + (x)) = 1$ and $k_x/(k_x + (x)) = 0$), then Equation 5 simplifies as:

$$r_k = \lambda\,(CH_2O) \quad (6)$$

which is a simple linear relation with the organic carbon concentration. This expression shows that if there are sufficient TEAs (and in general there is at least DIC), the total oxidation rate depends only on the dissolved organic carbon concentration. Of course, the relative contribution of each TEA to this oxidation still does depend on TEA concentrations, which is given by Equations 1–4.

2.2. The Partial Equilibrium Approach

The PEA assumes the oxidation of organic carbon to be kinetically controlled:

$$CH_2O + 2H_2O \rightarrow HCO_3^- + 5H^+ + 4e^-$$

whereas the reduction semi-reactions of the various TEAs are assumed to be in equilibrium (thus controlled by Gibbs free energy):

$$e^- + 0.25O_2 + H^+ \leftrightharpoons 0.5H_2O$$

$$e^- + 0.2NO_3^- + 1.2H^+ \leftrightharpoons 0.1N_2 + 0.6H_2O$$

$$e^- + Fe(OH)_3 + 3H^+ \leftrightharpoons Fe^{2+} + 3H_2O$$

$$e^- + 0.125HCO_3^- + 1.125H^+ \leftrightharpoons 0.125CH_4 + 0.375H_2O$$

Other non-redox equilibrium reactions can be added. Note that the approach assumes the electron activity (or pe) to be always in equilibrium with the redox couples of O_2/H_2O, NO_3^-/N_2, Fe^{3+}/Fe^{2+}, and HCO_3^-/CH_4 but not with organic carbon. The rate law for the oxidation of organic carbon (r_k) is often taken as the sum of Equations 1–4 (Greskowiak et al., 2006; Prommer et al., 2006; Rodríguez-Escales et al., 2017). This means that we can apply the same logic as for the fully kinetical approach. The rate law for r_k reduces to Equation 6 if we assume equal λ's ($\lambda_O = \lambda_N = \lambda_{Fe} = \lambda_C = \lambda$) and a sufficient amount of TEAs. However, unlike the fully kinetical approach, the oxidation rates by each TEA are not given by Equations 1–4. Instead, they must be deduced from mass balances of the various chemical species involved. This will be explained and illustrated in Sections 3 and 4 (particularly, Equation 12).

3. A Semi-Analytical Solution for the Partial-Equilibrium Approach

Here we will derive a semi-analytical solution of reactive transport assuming the partial-equilibrium approach described above and Equation 6 for the kinetic oxidation rate of organic carbon. The simplifications and the assumptions made in Equation 6 permit us to deduce an analytical solution including any number of aqueous reactions and precipitation-dissolution reactions of minerals in equilibrium if they are assumed to be ubiquitous in space. The deduction of our solution is based on the method described by De Simoni et al. (2005) and Sanchez-Vila et al. (2010). We will illustrate it by adding some more equilibrium reactions to the system described in Section 2.2. The first reaction is the oxidation of organic carbon:

$$Rk:\ CH_2O + 2H_2O \rightarrow HCO_3^- + 5H^+ + 4e^-$$

Following Equation 6, we assume a linear kinetic rate law for this reaction. The system has 11 equilibrium reactions including precipitation-dissolution of two minerals [$CaCO_3$(s) and amorphous $Fe(OH)_3$(s)]:

$$Re1:\ Ca^{2+} \leftrightharpoons CaCO_3(s) + H^+ - HCO_3^-$$

$$Re2:\ Fe(OH)_3(aq) \leftrightharpoons Fe(OH)_3(s)$$

$$Re3:\ O_2 \leftrightharpoons 2H_2O - 4H^+ - 4e^-$$

$$Re4:\ NO_3^- \leftrightharpoons 3H_2O - 6H^+ - 5e^- + 0.5N_2(aq)$$

$$Re5:\ Fe^{2+} \leftrightharpoons Fe(OH)_3(s) - 3H_2O + 3H^+ + e^-$$

$$Re6:\ FeCO_3(aq) \leftrightharpoons Fe(OH)_3(s) - 3H_2O + 2H^+ + e^- + HCO_3^-$$

$$Re7:\ CH_4 \leftrightharpoons -3H_2O + 9H^+ + 8e^- + HCO_3^-$$

$$Re8:\ OH^- \leftrightharpoons H_2O - H^+$$

$$Re9:\ CO_2(aq) \leftrightharpoons -H_2O + H^+ + HCO_3^-$$

$$Re10:\ Fe(OH)_4^- \leftrightharpoons Fe(OH)_3(s) + H_2O - H^+$$

$$Re11:\ Fe(OH)_2^+ \leftrightharpoons Fe(OH)_3(s) - H_2O + H^+$$

The equilibrium reactions are formulated in such a way that secondary species (on the left-hand side of $\leftrightharpoons$) can be considered to be composed of primary species (on the right-hand side). The primary species comprise the two minerals and H_2O, H^+, e^-, HCO_3^- and N_2. Although it is not common to use minerals as primary species, it greatly simplifies the decoupling procedure, because concentrations of aqueous species do not depend on those of minerals. For mathematical convenience, we write the stoichiometric coefficients in matrix form using subscripts "k" for kinetic reactions, "e" for equilibrium reactions, "m" for minerals, "a" for aqueous species (including

organic carbon), "*oc*" for organic carbon, *a*1 for primary aqueous species, and *a*2 for secondary aqueous species. For our chemical system this gives the following stoichiometric matrix (**S**):

$$\mathbf{S} = \begin{array}{|c|} \hline \mathbf{S}_k \\ \hline \mathbf{S}_e \\ \hline \end{array} = \begin{array}{|c|c|} \hline \mathbf{S}_{k,m} & \mathbf{S}_{k,a} \\ \hline \mathbf{S}_{e,m} & \mathbf{S}_{e,a} \\ \hline \end{array} = \begin{array}{|c|c|c|c|} \hline \mathbf{S}_{k,m} & \mathbf{S}_{k,a1} & \mathbf{S}_{k,oc} & \mathbf{S}_{k,a2} \\ \hline \mathbf{S}_{e,m} & \mathbf{S}_{e,a1} & \mathbf{S}_{e,oc} = \mathbf{0} & \mathbf{S}_{e,a2} = -\mathbf{I} \\ \hline \end{array}$$

$$= \begin{array}{c|cccccccccccc|c|cccccccccccc|} & & -2 & 5 & 4 & 1 & & -1 & & & & & & & & \\ \hline 1 & & & 1 & & -1 & & & -1 & & & & & & & \\ & 1 & & & & & & & & -1 & & & & & & \\ & & 2 & -4 & -4 & & & & & & -1 & & & & & \\ & & 3 & -6 & -5 & & 0.5 & & & & & -1 & & & & \\ & 1 & -3 & 3 & 1 & & & & & & & & -1 & & & \\ & 1 & -3 & 2 & 1 & 1 & & & & & & & & -1 & & \\ & & -3 & 9 & 8 & 1 & & & & & & & & & -1 & \\ & & 1 & -1 & & & & & & & & & & & & -1 \\ & & -1 & 1 & & 1 & & & & & & & & & & \\ & 1 & 1 & -1 & & & & & & & & & & & & \\ & 1 & -1 & 1 & & & & & & & & & & & & \\ \hline & CaCO$_3$(s) & Fe(OH)$_3$(s) & H$_2$O & H$^+$ & e$^-$ & HCO$_3^-$ & N$_2$(aq) & CH$_2$O & Ca^{2+} & Fe(OH)$_3$(aq) & O$_2$ & NO$_3^-$ & Fe^{2+} & FeCO3(aq) & CH$_4$ & OH$^-$ & CO$_2$(aq) & Fe(OH)$_4^-$ & Fe(OH)$_2^+$ & \end{array} \begin{array}{l} \text{Rk} \\ \text{Re1} \\ \text{Re2} \\ \text{Re3} \\ \text{Re4} \\ \text{Re5} \\ \text{Re6} \\ \text{Re7} \\ \text{Re8} \\ \text{Re9} \\ \text{Re10} \\ \text{Re11} \end{array} \quad (7)$$

Note that $\mathbf{S}_{e,oc} = \mathbf{0}$ and $\mathbf{S}_{e,a2} = -\mathbf{I}$. This comes from the fact that organic carbon is not involved in equilibrium reactions and that secondary species are considered to be composed of only primary species. Also note that $\mathbf{S}_{k,oc} = -1$ and $\mathbf{S}_{k,a2} = \mathbf{0}$. This is just a peculiarity of our chemical system. The mass balance equations for all species can be written, using vector-matrix notation, as:

$$\phi \frac{\partial \mathbf{c}}{\partial t} = \begin{pmatrix} 0 \\ (-\mathbf{q} \cdot \nabla \mathbf{c}_a + \nabla \cdot (\phi \mathbf{D} \nabla \mathbf{c}_a))^T \end{pmatrix} + \phi \mathbf{S}_k^T r_k + \phi \mathbf{S}_e^T \mathbf{r}_e \quad (8)$$

where $\mathbf{q}$ is the Darcy flux, ϕ is the porosity, $\mathbf{D}$ is a tensor for diffusion and/or dispersion, $\mathbf{r}_e$ is a vector of the rates of equilibrium reactions (in moles per volume of water per unit of time) and $\mathbf{c}$ a vector of concentrations of species (in moles per volume of water), that uses the same subscripts as the stoichiometric matrix [$\mathbf{c}^T = (\mathbf{c}_m\ \mathbf{c}_{a1}\ c_{oc}\ \mathbf{c}_{a2})^T = (\mathbf{c}_m\ \mathbf{c}_{a1}\ c_{oc}\ \mathbf{c}_{a2})^T$]. Note that only aqueous species include terms for advection and diffusion-dispersion. Contrary to kinetic reactions, rates of equilibrium reactions cannot be expressed directly through a rate law. Instead, a mass action laws for each equilibrium reaction has to be imposed (Equation 9).

$$\mathbf{S}_{e,a} \left(\log \mathbf{c}_a + \log \boldsymbol{\gamma}_a \right) = \log \mathbf{k} \quad (9)$$

As $\mathbf{S}_{e,oc} = \mathbf{0}$ and $\mathbf{S}_{e,a2} = -\mathbf{I}$ (Equation 7), these mass action laws can be rewritten as:

$$\log \mathbf{c}_{a2} = \mathbf{S}_{e,a1} \left(\log \mathbf{c}_{a1} + \log \boldsymbol{\gamma}_{a1} \right) - \log \boldsymbol{\gamma}_{a2} - \log \mathbf{k} \quad (10)$$

where $\boldsymbol{\gamma}$ is a vector of activity coefficients, that depend on the ionic strength of the solution, and $\log \mathbf{k}$ is the equilibrium constant of the reaction. Note that concentrations of minerals do not affect (9) or (10), because their activities equal unity.

An important remark has to be made here on the electron, e^-. Its concentration reflects the redox potential and is not an actual concentration of free e^- dissolved in water. Nevertheless, we assume a virtual concentration of e^- although its concentration is in reality 0. The transport and storage terms of Equation 8 are negligible with respect to reaction rates. Therefore, rather than Equation 8, the mass balance of e^- for our chemical system has to be expressed as:

$$0 = 4r_k - 4r_{e3} - 5r_{e4} + r_{e5} + r_{e6} + 8r_{e7} \Rightarrow r_k = r_{e3} + 1.25r_{e4} - 0.25\,(r_{e5} + r_{e6}) - 2r_{e7} \quad (11)$$

We can use Equation 11 to distinguish between rates of aerobic oxidation (r_O), denitrification (r_N), iron reduction (r_{Fe}) and methanogenesis (r_C). It would be natural to define these rates by:

$$\begin{aligned} r_O &= r_{e3} \\ r_N &= 1.25r_{e4} \\ r_{Fe} &= -0.25\,(r_{e5} + r_{e6}) \\ r_C &= -2r_{e7} \end{aligned} \quad (12)$$

which, of course, means that $r_k = r_O + r_N + r_{Fe} + r_C$

We usually simplify mass balance Equation 8 by multiplying them with a $(N_s - N_e) \times N_s$ component matrix $\mathbf{U}$ (N_s being the number of species, N_e the number of equilibrium reactions). Matrix $\mathbf{U}$ (also called kernel or null space) eliminates the rates of equilibrium reactions ($\mathbf{r}_e$). By definition $\mathbf{U}\mathbf{S}_e^T = 0$. For our semi-analytical solution, we subdivide $\mathbf{U}$ into three other component matrices:

1. A component matrix for minerals ($\mathbf{U}_{mc}$) that eliminates both equilibrium and kinetic reactions. Its number of rows equals the number of minerals. It is constructed by using the minerals as base columns.
2. An aqueous conservative component matrix ($\mathbf{U}_{ac}$). It contains only aqueous species and also eliminates both equilibrium and kinetic reactions. Its number of rows equals the number of aqueous species minus the rank of matrix $\mathbf{S}_a$, which equals the number of equilibrium plus kinetic reactions. Therefore, the number of aqueous conservative components (N_{ac}) or rows of $\mathbf{U}_{ac}$ equals $N_{ac} = N_a - N_e - N_k = N_a - N_e - 1$ (N_a being the number of aqueous species and N_k the number of kinetic reactions, which equals one). It is constructed by using as base columns the primary species excluding CH_2O and minerals.
3. A component matrix for organic carbon $\mathbf{U}_{oc}$. It has one row, and its elements are all zero except the one referring to CH_2O, which has a value of one. As the equilibrium reactions do not involve CH_2O, it eliminates $\mathbf{r}_e$ (i.e., $\mathbf{U}_{oc}\mathbf{S}_e^T = 0$) but not $\mathbf{r}_k$ ($\mathbf{U}_{oc}\mathbf{S}_k^T \neq 0$).

For our chemical system this gives the following:

$$\mathbf{U} = \begin{bmatrix} \mathbf{U}_{mc} \\ \mathbf{U}_{ac} \\ \mathbf{U}_{oc} \end{bmatrix} = \begin{bmatrix} \mathbf{I} & \mathbf{U}_{mc,a} \\ \mathbf{0} & \mathbf{U}_{ac,a} \\ \mathbf{0} & \mathbf{U}_{oc,a} \end{bmatrix} = \begin{bmatrix} \mathbf{I} & \mathbf{0} & -\left(\mathbf{S}_{e,m}^T\mathbf{S}_{k,a2}^T + \mathbf{S}_{k,m}^T\right)\left(\mathbf{S}_{k,oc}^T\right)^{-1} & \mathbf{S}_{e,m}^T \\ \mathbf{0} & \mathbf{I} & -\left(\mathbf{S}_{e,a1}^T\mathbf{S}_{k,a2}^T + \mathbf{S}_{k,a1}^T\right)\left(\mathbf{S}_{k,oc}^T\right)^{-1} & \mathbf{S}_{e,a1}^T \\ \mathbf{0} & \mathbf{0} & 1 & \mathbf{0} \end{bmatrix}$$

$$= \left[\begin{array}{cccccccc|c|ccccccccccc} 1 & & & & & & & & & 1 & & & & & & & & & \\ & 1 & & & & & & & & & 1 & & & 1 & 1 & & & & 1 & 1 \\ & & 1 & & & & & & & -2 & & 2 & 3 & -3 & -3 & -3 & 1 & -1 & 1 & -1 \\ & & & 1 & & & & & & 5 & 1 & -4 & -6 & 3 & 2 & 9 & -1 & 1 & -1 & 1 \\ & & & & 1 & & & & & 4 & & -4 & -5 & 1 & 1 & 8 & & & & \\ & & & & & 10 & & & & 1 & -1 & & & & 1 & 1 & & 1 & & \\ & & & & & & 1 & & & & & & & 0.5 & & & & & & \\ & & & & & & & & & 1 & & & & & & & & & & \end{array}\right] \quad (13)$$

$CaCO_3(s)$ $Fe(OH)_3(s)$ H_2O H^+ e^- HCO_3^- N_2 CH_2O Ca^{2+} $Fe(OH)_3(aq)$ O_2 NO_3^- Fe^{2+} $FeCO3(aq)$ CH_4 OH^- $CO_2(aq)$ $Fe(OH)_4^-$ $Fe(OH)_2^+$

where the column referring to e^- has to be made 0 (indicated in red) because in reality, the concentration of e^- is 0. Some rows in $\mathbf{U}$ have a clear meaning. For instance, the first row represents the component Ca, the second row Fe, the fifth the reduction capacity, and the seventh the component N. The meaning of other rows is less obvious. Multiplying this component matrix by Equation 8 gives:

$$\phi\frac{\partial \mathbf{c}_m}{\partial t} + \phi\frac{\partial \mathbf{u}_{mc,a}}{\partial t} = \left(-\mathbf{q}\cdot\nabla\mathbf{u}_{mc,a} + \nabla\cdot\left(\phi\mathbf{D}\nabla\mathbf{u}_{mc,a}\right)\right)^T \quad (14)$$

$$\phi\frac{\partial \mathbf{u}_{ac}}{\partial t} = \left(-\mathbf{q}\cdot\nabla\mathbf{u}_{ac} + \nabla\cdot\left(\phi\mathbf{D}\nabla\mathbf{u}_{ac}\right)\right)^T \quad (15)$$

$$\phi\frac{\partial c_{oc}}{\partial t} = -\mathbf{q}\cdot\nabla c_{oc} + \nabla\cdot\left(\phi\mathbf{D}\nabla c_{oc}\right) + \phi\mathbf{S}_{k,oc}^T r_k \quad (16)$$

where $\mathbf{u}_{mc,a} = \mathbf{U}_{mc,a}\mathbf{c}_a$ and $\mathbf{u}_{ac} = \mathbf{U}_{ac}\mathbf{c}_a$ are vectors of concentrations of dissolved minerals and aqueous conservative components. For our chemical system we use a linear kinetic rate (Equation 6) and $\mathbf{S}_{k,om} = -1$ (Equation 7). Then, Equation 16 becomes:

$$\phi\frac{\partial c_{oc}}{\partial t} = -\mathbf{q}\cdot\nabla c_{oc} + \nabla\cdot\left(\phi\mathbf{D}\nabla c_{oc}\right) - \phi\lambda c_{oc} \quad (17)$$

which is a simple advection-dispersion equation with linear decay. All concentrations and reaction rates can be calculated by the following procedure:

Table 1
Chemical Composition of the Inlet Water and Parameters for Both Examples

Chemical composition of inlet water		
pH		8.16
O_2		2.55×10^{-4} M
Total N		1.00×10^{-3} M
Total Fe		2.56×10^{-8} M
DIC		7.64×10^{-4} M
Total Ca		8.83×10^{-4} M
CH_2O		2.50×10^{-3} M
Kinetic rate parameters	**This work**	**Literature range[a]**
$\lambda\ (d^{-1})$[b]	0.1	1×10^{-4}–1×10^{-1}
$k_{O_2}(M)$[c]	1.0×10^{-5}	1×10^{-6}–1×10^{-4}
$k_{NO_3^-}(M)$[c]	1.0×10^{-5}	1×10^{-6}–1×10^{-4}
$k_{FeIII}(M)$[c]	1.0×10^{-8}	0–1×10^{-4}
$k_{DIC}(M)$[c]	1.0×10^{-5}	1×10^{-6}–1×10^{-4}

[a]Brun & Engesgaard, 2002; Greskowiak et al., 2006; Rolle et al., 2008. [b]used in all models (Section 4.3, 4.4, and 4.5). [c]used in the fully kinetic models (Section 4.5).

1. Calculate $\mathbf{u}_{ac}$ by solving Equation 15. For this, one can use existing analytical solutions (e.g., van Genuchten and Alves, 1982). Alternatively, one can also use numerical solutions.
2. Calculate c_{oc} by solving Equation 16 or 17. Analytical or numerical solutions exist for this also, at least for Equation 17.
3. Calculate concentrations of all other aqueous species from $\mathbf{u}_{ac}$ and c_{oc} by solving the mass action laws (9) together with the definition of $\mathbf{u}_{ac}$ ($\mathbf{u}_{ac} = \mathbf{U}_{ac}\mathbf{c}_a$). In general, no analytical solutions exist and they can be solved numerically by standard chemical speciation codes such as Phreeqc (Parkhurst & Appelo, 1999). The kinetic reaction rate can be calculated straightforwardly from Equation 5 or 6.
4. If all concentrations and the kinetic reaction rate are known, we can calculate the rates of equilibrium reactions ($\mathbf{r}_e$) from the mass balance Equation 8 of the secondary species:

$$\phi\frac{\partial \mathbf{c}_{a2}}{\partial t} = (-\mathbf{q}\cdot\nabla\mathbf{c}_{a2} + \nabla\cdot(\phi\mathbf{D}\nabla\mathbf{c}_{a2}))^T + \phi\mathbf{S}_{k,a2}^T r_k + \phi\mathbf{S}_{e,a2}^T\mathbf{r}_e \tag{18}$$

As the equilibrium reactions write the secondary species explicitly as a function of primary species, $\mathbf{S}_{e2} = -\mathbf{I}$ (Equation 7), Equation 18 can be rewritten as:

$$\mathbf{r}_e = -\frac{\partial \mathbf{c}_{a2}}{\partial t} + (-\mathbf{v}\cdot\nabla\mathbf{c}_{a2} + \nabla\cdot(\mathbf{D}\nabla\mathbf{c}_{a2}))^T + \mathbf{S}_{k,a2}^T r_k \tag{19}$$

where $\mathbf{v}$ is the porewater velocity ($\mathbf{v} = \phi^{-1}\mathbf{q}$). As $\mathbf{c}_{a2}$ is a function of only $\mathbf{u}_c$ and c_{oc}, we can write:

$$\begin{aligned}\mathbf{r}_e = {} & \frac{\partial \mathbf{c}_{a2}}{\partial \mathbf{u}_{ac}}\left[-\frac{\partial \mathbf{u}_{ac}}{\partial t} + (-\mathbf{v}\cdot\nabla\mathbf{u}_{ac} + \nabla\cdot(\mathbf{D}\nabla\mathbf{u}_{ac}))^T\right] + \sum_i \frac{\partial^2 \mathbf{c}_{a2}}{\partial u_{ac,i}^2}\nabla^T u_{ac,i}\mathbf{D}\nabla u_{ac,i} \\ & + \frac{\partial \mathbf{c}_{a2}}{\partial c_{oc}}\left[-\frac{\partial c_{oc}}{\partial t} - \mathbf{v}\cdot\nabla c_{oc} + \nabla\cdot(\mathbf{D}\nabla c_{oc})\right] + \frac{\partial^2 \mathbf{c}_{a2}}{\partial c_{om}^2}\nabla^T c_{oc}\mathbf{D}\nabla c_{oc} + \mathbf{S}_{k,a2}^T r_k\end{aligned} \tag{20}$$

Substitution of Equations 15 and 16 into 20 yields:

$$\mathbf{r}_e = \sum_i \frac{\partial^2 \mathbf{c}_{a2}}{\partial u_{ac,i}^2}\nabla^T u_{ac,i}\mathbf{D}\nabla u_{ac,i} + \frac{\partial^2 \mathbf{c}_{a2}}{\partial c_{oc}^2}\nabla^T c_{oc}\mathbf{D}\nabla c_{oc} + \left(\mathbf{S}_{k,a2}^T - \frac{\partial \mathbf{c}_{a2}}{\partial c_{oc}}\mathbf{S}_{k,oc}^T\right) r_k \tag{21}$$

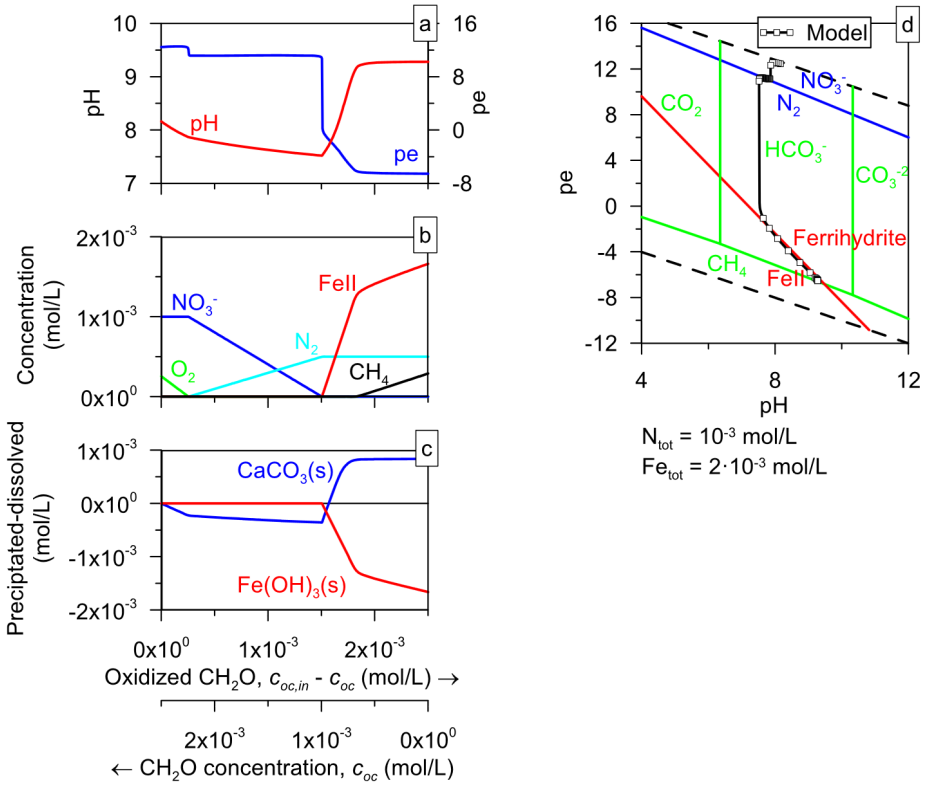

Figure 1. Results of the batch calculations by Phreeqc: pH and pe (a), aqueous concentrations (b), minerals (c) and pe-pH diagram (d). Figures a, b and c have two horizontal axes: oxidized CH_2O and CH_2O concentrations. In figure (c), positive values refer to precipitation and negative to dissolution. In figure (d), each square represents an additional amount of oxidized organic carbon of 5×10^{-5} mol/L.

From $\mathbf{r}_e$, we can also obtain r_O, r_N, r_{Fe}, and r_C through Equation 12. The derivatives ($\partial^2\mathbf{c}_{a2}/\partial u_{ac,i}^2$, $\partial\mathbf{c}_{a2}/\partial c_{oc}$ and $\partial^2\mathbf{c}_{a2}/\partial c_{oc}^2$) can be obtained numerically from the results of step 3. Gradients $\nabla u_{ac,i}$ and ∇c_{oc} must be deduced from the analytical or numerical solutions of step 1 and 2. Note that the first two terms on the right-hand side of 21 are identical to those obtained by De Simoni et al. (2007). In addition, we have another term for kinetic reaction rates.

5. Similarly to Equation 21, we can calculate the concentration of minerals or their precipitation-dissolution rates:

$$\frac{\partial \mathbf{c}_m}{\partial t} = \sum_i \frac{\partial^2 \mathbf{u}_{mc,a}}{\partial u_{ac,i}^2} \nabla^T u_{ac,i} \mathbf{D} \nabla u_{ac,i} + \frac{\partial^2 \mathbf{u}_{mc,a}}{\partial c_{oc}^2} \nabla^T c_{oc} \mathbf{D} \nabla c_{oc} - \frac{\partial \mathbf{u}_{mc,a}}{\partial c_{oc}} \mathbf{S}_{k,oc}^T r_k \tag{22}$$

4. Applications of the Semi-Analytical Solution

In this section, we apply the semi-analytical solution to two very simple examples. The first one has only advection (Section 4.3) and the second one only diffusion (Section 4.4). For both examples, the concentrations of the aqueous conservative components ($\mathbf{u}_{ac}$) are constant, but the concentration of the organic carbon (c_{oc}) changes as a result of oxidation. Besides this, we also verify our solution by comparing it with a Phreeqc numerical model also including organic carbon oxidation assuming PEA. First (Section 4.2), we calculate the chemical composition as a function of the concentration of organic carbon (c_{oc}), following the procedure described in Section 3 (step 3). All the parameters needed for the calculations are presented in Section 4.1.

4.1. Chemical Model

We used the Phreeqc code (Parkhurst & Appelo, 1999) to calculate the chemical compositions. Thermodynamic data were taken from the Phreeqc database (phreeqc.dat), from which we removed ammonium to avoid the

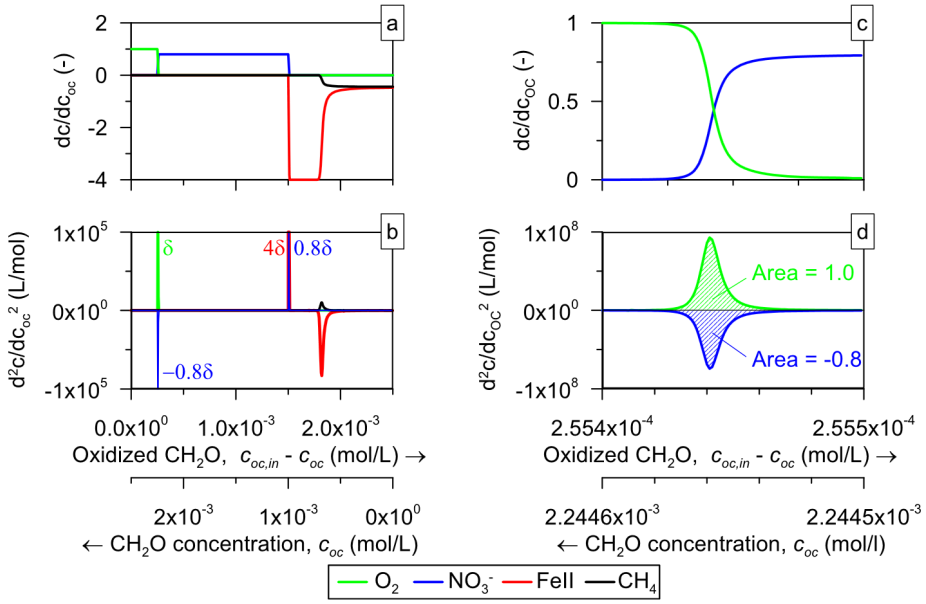

Figure 2. First (figure a and c) and second (figures b and d) derivatives of the concentrations of secondary species with respect to concentration of organic carbon. All have two horizontal axes: oxidized CH_2O and CH_2O concentrations. In figure (b) δ is the Dirac delta function of Equation 23 and Table 2. Figure (c) is an enlargement of figure a near the O_2/NO_3^- front with a smaller scale for the horizontal and vertical axes. Likewise, figure (b) has a smaller scale than figure d for the horizontal axis, but a larger scale for the vertical axis. It can be verified that the areas of figure (d) agree with $\boldsymbol{\alpha}_f$ in Table 2.

unrealistic reduction of NO_3^- and N_2 to NH_4^+. Table 1 shows the chemical composition of the inlet water together with the kinetic rate parameters, to be used later in the applications. The water at the inlet is in equilibrium with $CaCO_3$(s), $Fe(OH)_3$(s), and gas with a partial pressure for O_2 of 0.2 bar and for CO_2 of $10^{-3.5}$ bar. All redox couples, except that of CH_2O/HCO_3^-, are assumed at equilibrium. As the water is aerobic, concentrations of N_2, Fe^{2+}, and CH_4 are practically 0. The constant concentrations of the conservative components ($\mathbf{u}_{ac}$) can be calculated from this chemical composition. We use the same chemical elements and minerals as the chemical system of Section 3. However, as Phreeqc incorporates all possible aqueous complexes from its database, there may be more equilibrium reactions than the system of Section 3.

4.2. Batch Calculations

The batch model consists of adding to the inlet water of Table 1 incremental amounts of CH_2O that are subsequently oxidized. Figure 1 shows the results of these Phreeqc batch calculations. Note that when the organic carbon concentration is high, the amount of oxidized organic carbon is low, and, therefore, the concentrations of TEAs are high. Clearly, different redox zones can be distinguished. O_2 concentrations drop with increasing oxidized organic carbon in an O_2 redox zone (Figure 1b). Then, NO_3^- concentrations drop and those of N_2 increase in a NO_3^- redox zone, followed by an increase in Fe(II) in a Fe redox zone. Finally, there is a zone of both Fe reduction and CH_4 genesis with increasing Fe(II) and CH_4 concentrations. These zones are also reflected by pe and pH (Figure 1a). As expected, pe drops for each subsequent redox zone. Aerobic oxidation produces protons, which lowers the pH in the O_2 redox zone (see chemical reactions in Section 2.1). The same occurs for denitrification though to a lesser extent. Iron reduction consumes protons, which increases the pH. There is no proton production or consumption at the zone of Fe reduction and CH_4 genesis and pH is kept constant. $CaCO_3$(s) reacts to changes in pH with dissolution when protons are produced and precipitation when protons are consumed (Figure 1d). Aerobic oxidation, denitrification, and iron reduction are clearly separated. However, there is no clear separation between iron reduction and methanogenesis. This can be explained by the pe-pH diagram (Figure 1c). Starting with high O_2 and organic carbon concentrations pe-pH values are near the H_2O/O_2 line. When more CH_2O is oxidized, pe-pH values reach the NO_3^-/N_2 line (blue) in the NO_3^- redox zone. This is followed by a drop to the FeII/$Fe(OH)_3$(s) line (red) in the Fe redox zone. As the FeII/$Fe(OH)_3$(s) line crosses the CH_4/HCO_3 line (green), the water reaches the intersection point and remains there producing both Fe(II) and CH_4. It can be questioned

Table 2
Parameters for Equation 23

		Redox front (f)	
		O_2/NO_3	NO_3/Fe
$c_{om,f}$ (mol/L)		2.24×10^{-3}	9.95×10^{-4}
$\boldsymbol{\alpha}_f$	O_2	1.0	0.0
	NO_3^-	−0.8	0.8
	FeII	0.0	4.0
	CH_4	0.0	0.0

whether this occurs in reality. There may be other minerals, such as siderite ($FeCO_3$), not considered in our chemical system, that can change the pe-pH diagram. We did not consider this mineral, because our analytical solution only permits minerals that are present ubiquitously and siderite is only stable at zones with low redox potential (Stumm & Morgan, 1996, Chapter 8.4). Nevertheless, co-occurrence of Fe reduction and methanogenesis have been found in laboratory studies though not for amorphous $Fe(OH)_3$(s) but for other Fe(III) oxides, such as hematite and magnetite (Zhou et al., 2014).

Our analytical solution also requires first and second derivatives with respect to c_{oc}, shown in Figure 2. First derivatives follow the stoichiometry of the different oxidation reactions in the different redox zones, which we can characterize by:

$$\text{Rk} + \text{Re3}: \ CH_2O + O_2 \rightarrow HCO_3^- + H^+$$

$$\text{Rk} + 0.8\text{Re4}: \ CH_2O + 0.8NO_3^- \rightarrow HCO_3^- + 0.4N_2 + 0.4H_2O + 0.2H^+$$

$$\text{Rk} + 4\text{Re5}: \ CH_2O + 4Fe(OH)_3 + 7H^+ \rightarrow HCO_3^- + 4Fe^{2+} + 10H_2O$$

$$\text{Rk} + 0.5\text{Re7}: \ CH_2O + 0.5H_2O \rightarrow 0.5HCO_3^- + 0.5CH_4 + 0.5H^+$$

Note that there are very abrupt changes in first derivatives at an O_2/NO_3^- and NO_3^-/Fe^{3+} redox front. The O_2/NO_3^- front is located at the CH_2O concentration equal to the inlet CH_2O concentration minus the O_2 concentration of Table 1 ($2.50 \times 10^{-3} - 2.55 \times 10^{-4} = 2.24 \times 10^{-3}$ mol/L) and the NO_3^-/Fe redox front at that equal to the inlet CH_2O concentration minus the O_2 concentration minus 0.8 times NO_3^- concentration ($2.50 \times 10^{-3} - 2.55 \times 10^{-4} - 0.8 \times 1.0 \times 10^{-3} = 9.95 \times 10^{-4}$ mol/L). There is no clear Fe/CH_4 front due to the already discussed co-occurrence of Fe reduction and methanogenesis. The sharp fronts mean very high second derivatives at the O_2/NO_3^- and NO_3^-/Fe redox front (Figure 2b). As can be seen in Figures 2c and 2d, the width of the O_2/NO_3^- front is around 10^{-8} mol/L, compared to an initial organic carbon concentration of 2.5×10^{-3} mol/L. The size of the NO_3^-/Fe redox front is similarly small. These thin fronts justify the use of the Dirac delta function to approximate the second derivatives:

$$\frac{\partial^2 \mathbf{c}_{2a}}{\partial c_{oc}^2} = \delta\left(c_{om} - c_{om,f}\right)\boldsymbol{\alpha}_f \quad f = O_2/NO_3^-, NO_3^-/Fe^{3+} \tag{23}$$

where subscript f refers to the redox front, δ is the Dirac delta function, $c_{oc,f}$ the front location in terms of organic carbon concentration and $\boldsymbol{\alpha}$ is a vector containing jumps in first derivatives. Table 2 shows the values for $c_{oc,f}$ and $\boldsymbol{\alpha}$.

4.3. Application 1: 1D Steady State With Only Advection

The first model assumes a one-dimensional domain with homogeneous water flow, porosity and decay constant (λ) and with advection as the only transport process. Then, the mass balance equation of organic carbon becomes:

$$0 = -v\frac{\partial c_{oc}}{\partial x} - \lambda c_{oc} \tag{24}$$

where v is the porewater velocity. Note that by using porewater velocity in stead of Darcy flux, the porosity is not required. The solution of Equation 24 is:

$$c_{oc} = c_{oc,in} exp\left(\frac{-\lambda x}{v}\right) \tag{25}$$

where $c_{oc,in}$ is the concentration of organic carbon at the inlet. The model uses a porewater velocity (v) of 1.0 m/day. Its length is 30 m.

As stated above, our semi-analytical solution is also verified by comparing it with a numerical solution, calculated with Phreeqc. The organic carbon oxidation scheme is also based on the PEA calculated with the same

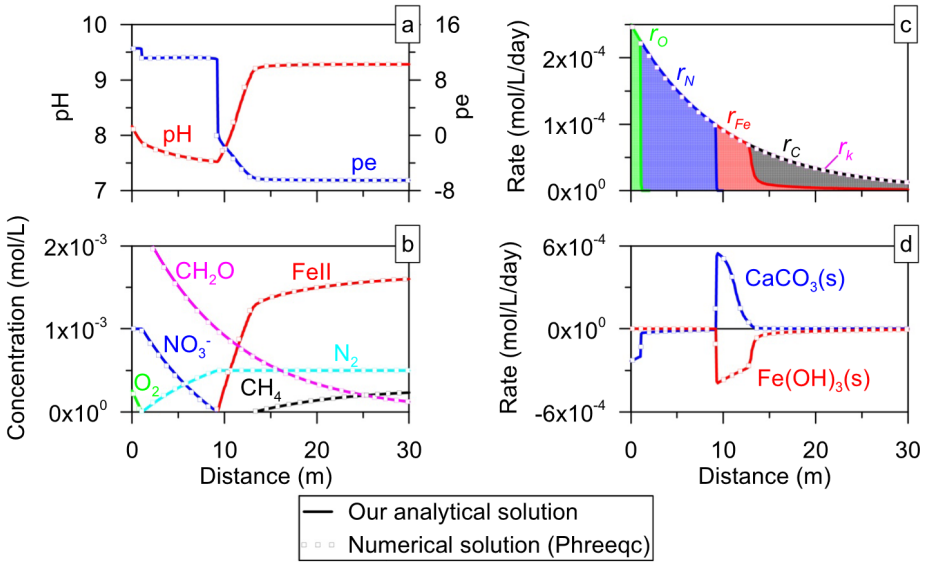

Figure 3. Results of the advection model calculated by the semi-analytical model (lines) and the numerical model of Phreeqc (squares). Figure (c) is a stacked graph for r_O, r_N, r_{Fe}, and r_C. The total organic carbon oxidation rate ($r_O + r_N, + r_{Fe} + r_C$) equals r_k, calculated by Phreeqc. In Figure (d) positive rates refer to precipitation and negative to dissolution.

initial conditions and parameters as our analytical solution (Table 1). The total length is divided into 100 cells of 0.3 m. As Phreeqc does not allow steady state calculations, we used a transient state model with a total time of 60 days divided into 200 time steps. At this total time, the system will have reached a steady state, because it is two times the transient time defined as length of the domain divided by velocity (30 m/1.0 m/day = 30 days). Therefore, we used the results of the last time step for comparison with the steady state analytical model.

Figure 3 shows the results of the advection model. Those for the analytical and the numerical model are close to identical, which verifies the correct calculation of the analytical solution. The aqueous chemistry (Figures 3a and 3b) is very similar to Figures 1a and 1b except for the horizontal axis that is not oxidized organic carbon but distance. The reason is that concentrations of solutes only depend on aqueous component concentrations ($\mathbf{u}_{ac}$) and concentrations of organic carbon (c_{oc}) as explained in step 3 of our procedure. As in our case $\mathbf{u}_{ac}$ is constant, solute concentrations only depend on c_{oc}, which in turn depends on distance through Equation 25. In effect Equation 25 expresses the transformation of the horizontal axis of Figures 1a and 1b (organic carbon concentration) into that of Figures 3a and 3b (distance). We can also calculate the reactions rates by applying Equations 21 and 22. In our case $\mathbf{D} = 0$ and, for our particular chemical system of Equation 7, $\mathbf{u}_{ac}$ is constant, $\mathbf{S}_{k,om} = -1$ and $\mathbf{S}_{k,a2} = 0$. This leads to:

$$\mathbf{r}_e = \frac{\partial \mathbf{c}_{a2}}{\partial c_{oc}} r_k \tag{26}$$

$$\frac{\partial \mathbf{c}_m}{\partial t} = \frac{\partial \mathbf{u}_{mc,a}}{\partial c_{oc}} r_k \tag{27}$$

Figures 3c and 3d show the rates of organic carbon oxidation by the various TEAs, obtained from $\mathbf{r}_e$ and Equation 12, and the precipitation-dissolution rates of the two minerals. Upstream, organic carbon is oxidized aerobically, followed by denitrification, iron reduction and methanogenesis. Aerobic oxidation, denitrification, and iron reduction are separated by clear fronts, but there is no clear front between iron reduction and methanogenesis. $Fe(OH)_3(s)$ dissolution is directly related to iron reduction. In the aerobic oxidation zone $CaCO_3(s)$ dissolves because of the proton formation of reaction Rk + Re3. There is less proton formation during denitrification (Rk + 0.8Re4) and, hence, less dissolution. Iron reduction (Rk + 4Re4) consumes protons and causes $CaCO_3(s)$ to precipitate.

4.4. 1D Steady State With Only Diffusion

The mass balance equation of organic carbon in a one-dimensional domain and with only diffusion at steady state is:

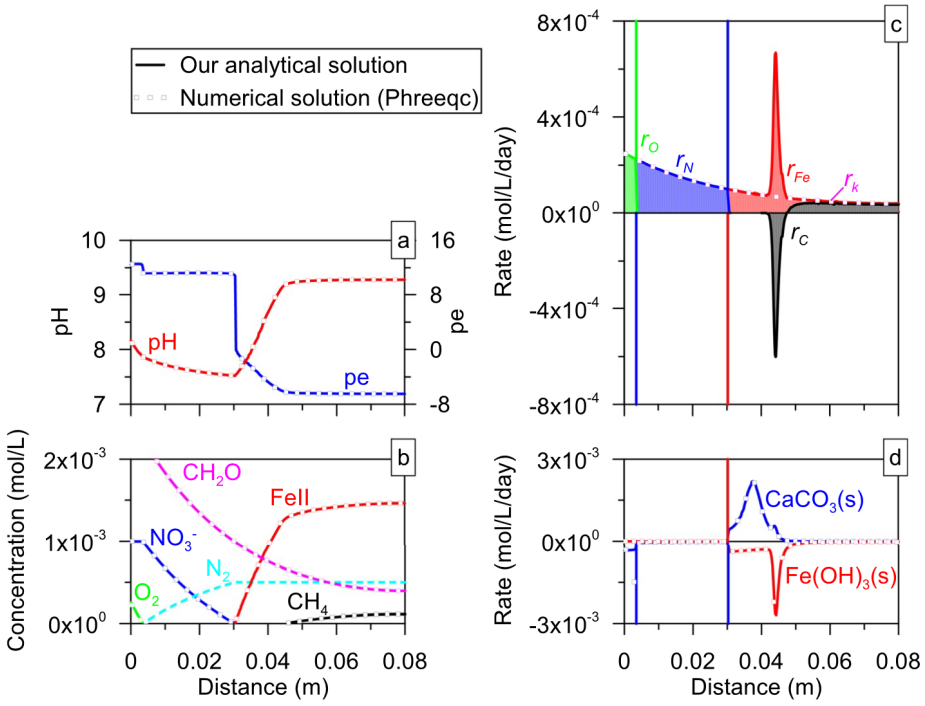

Figure 4. Results of the diffusion model calculated by the analytical model (lines) and the numerical model of Phreeqc (squares). The vertical lines in figure c and d indicate values that go to infinity. Figure (c) is a stacked graph for r_O, r_N, r_{Fe}, and r_C. The total organic carbon oxidation rate ($r_O + r_N, + r_{Fe} + r_C$) equals r_k, calculated by Phreeqc. In figure (d) positive rates refer to precipitation and negative to dissolution.

$$0 = D\frac{\partial^2 c_{oc}}{\partial x^2} - \lambda c_{oc} \tag{28}$$

with boundary conditions

$$\begin{aligned} c_{oc} &= c_{oc,in} \quad x = 0 \\ \frac{\partial c_{oc}}{\partial x} &= 0 \quad x = L \end{aligned} \tag{29}$$

where $c_{oc,in}$ is the concentration of organic carbon at the inlet and L is the length of the domain. Like the advection model, porosity is not required. The solution is:

$$c_{oc} = c_{oc,in}\frac{exp\left(\frac{x-L}{x_C}\right) + exp\left(-\frac{x-L}{x_C}\right)}{exp\left(\frac{L}{x_C}\right) + exp\left(-\frac{L}{x_C}\right)} \tag{30}$$

$$\frac{\partial c_{oc}}{\partial x} = \frac{c_{oc,in}}{x_C}\frac{exp\left(\frac{x-L}{x_C}\right) - exp\left(-\frac{x-L}{x_C}\right)}{exp\left(\frac{L}{x_C}\right) + exp\left(-\frac{L}{x_C}\right)} \tag{31}$$

where $x_C = \sqrt{D/\lambda}$ is a characteristic length. The model uses a diffusion coefficient (D) of 1.0×10^{-4} m^2/day (=1.2×10^{-9} m^2/s) and a length (L) of 0.08 m.

Like the advection model, we compared our analytical solution with a numerical solution, calculated with Phreeqc. The total length is divided into 100 cells. Total time is 100 days divided into 200 time steps. This is sufficient for the system to reach a steady state, defined as about three times the characteristic time for diffusion in the domain [$=L^2/(2D) = 32$ days].

Reaction rates can be calculated by applying Equation 21, similarly to the advection model but with an additional term for diffusion:

$$\mathbf{r}_e = \frac{\partial^2 \mathbf{c}_{a2}}{\partial c_{oc}^2} D \left(\frac{dc_{oc}}{dx} \right)^2 + \frac{\partial \mathbf{c}_{a2}}{\partial c_{oc}} r_k \tag{32}$$

$$\frac{\partial \mathbf{c}_m}{\partial t} = \frac{\partial^2 \mathbf{u}_{mc,a}}{\partial c_{oc}^2} D \left(\frac{dc_{oc}}{dx} \right)^2 + \frac{\partial \mathbf{u}_{mc,a}}{\partial c_{oc}} r_k \tag{33}$$

Figure 4 shows the results of the calculation. The aqueous chemistry (Figures 4a and 4b) shows a very similar pattern to Figures 1a and 1b and Figures 3a and 3b and does not require further discussion. Like the advection model, the aqueous chemistry of the analytical and numerical model of Phreeqc is near identical. However, the reaction rates (Figures 4c and 4d) have some interesting features. Although the total oxidation of organic carbon by all TEAs (r_k) drops gradually, the aerobic oxidation (r_O) and denitrification (r_N) show huge upward and downward spikes at the O_2/NO_3 front. These spikes are a result of the diffusion term with second derivatives of Equation 32. If Dirac delta functions of Equation 23 are assumed for these second derivatives, these spikes go to positive and negative infinities. This means an infinite organic carbon oxidation by O_2 together with an infinite organic carbon formation by oxidizing N_2 to NO_3^-. The same happens with denitrification and iron reduction at the NO_3^-/Fe front. As there is no abrupt Fe/CH_4 front, there are no infinite rates here, but still there are considerable spikes in the rates of iron reduction and (negative) methanogenesis. Rather than simultaneous organic carbon decay and formation by different TEAs, it is better to represent the chemistry at the fronts by the following reactions:

$$O_2/NO_3^- \text{ front: } O_2 + 0.4N_2 + 0.4H_2O \rightarrow 0.8NO_3^- + 0.8H^+$$

$$NO_3^-/Fe \text{ front: } 0.8NO_3^- + 4Fe^{2+} + 9.6H_2O \rightarrow 0.4N_2 + 4Fe(OH)_3(s) + 7.2H^+$$

$$Fe/CH_4 \text{ front: } 4Fe(OH)_3(s) + 0.5CH_4 + 7.5H^+ \rightarrow 4Fe^{2+} + 0.5HCO_3^- + 10.5H_2O$$

Looking at the gradients of concentrations O_2, N_2 and NO_3^- (Figure 4b), we can infer that O_2 and N_2 diffuses toward the O_2/NO_3^- front without diffusing away from it. On the other hand, NO_3^- only diffuses away from this front. This means that there must be a sink for O_2 and N_2 and a source for NO_3^-. This is provided for by the above oxidation of N_2 by O_2 to NO_3^-, which the PEA assumes to be in equilibrium. Similar analyses can be made for the NO_3^-/Fe and Fe/CH_4 fronts, where FeII is oxidized by NO_3^- and CH_4 is oxidized by $Fe(OH)_3$(s), respectively. Of course, the oxidation of N_2 by O_2 does not occur in reality. In fact, it motivated Brun and Engesgaard (2002) to treat this reaction as kinetic. This is clearly one of the main limitations of the PEA. As it assumes thermodynamic equilibrium for all TEAs, all thermodynamically favorable reactions will occur. Note that this shortcoming is only relevant for transport cases dominated by diffusion and not for cases where advection is the main transport process and that do not show spikes in reaction rates. Nonetheless, FeII can be oxidized by NO_3^-, which is a process mediated by lithoautotrophic microorganisms (Torrentó et al., 2010).

At this point, we can use our analytical solution to further analyze the impact of this shortcoming. The reaction rates at the O_2/NO_3^- and NO_3^-/Fe fronts go to infinity or, at least, to very high values in a very narrow space, which is difficult to quantify. However, the reaction rates integrated over distance at these fronts do not go to infinity. We can see this by integrating the diffusion term of Equation 32 over an infinitely small distance ($\Delta x \rightarrow 0$) around the front position (x_f). This yields the following equation:

$$\int_{x_f-\Delta x}^{x_f+\Delta x} \frac{\partial^2 \mathbf{c}_{a2}}{\partial c_{oc}^2} D \left(\frac{dc_{oc}}{dx} \right)^2 dx = \int_{c_f-\Delta x \frac{dc_{oc}}{dx}}^{c_f+\Delta x \frac{dc_{oc}}{dx}} \delta \left(c_{oc} - c_f \right) D \frac{dc_{oc}}{dx} dc_{oc} \, \boldsymbol{\alpha}_f = D \left| \frac{dc_{oc}}{dx} \right| \boldsymbol{\alpha}_f \tag{34}$$

Table 3 shows the results of Equation 34 and compares them with other terms in the mass balances of the main redox species. As can be seen, the masses of solutes reacting at the fronts are by no means small in comparison to those reacting elsewhere or diffusing into the domain at the inlet. Moreover, NO_3^-, FeII, and CH_4 cannot diffuse into or out of the domain due to the zero gradient at the inlet, which means that formation and consumption of these species always compensate each other.

Table 3
Mass Balances of the Main Redox Species for the Diffusion Model

Process	Location	x (mm)	Mass balance (mmol m^{-2} day^{-1}) CH_2O	O_2	NO_3^-	FeII	CH_4
Influx diffusion	Inlet	0.0	7.81	7.81	0	0	0
Rk + Re3	O_2 zone	0.0–3.5	−0.82	−0.82	0	0	0
Re3 − 0.8Re4	O_2/NO_3^- front	3.5	0	−6.99	5.59	0	0
Rk + 0.8Re4	NO_3^- zone	3.5–30.3	−4.10	0	−3.28	0	0
0.8Re4 − 4Re5	NO_3^-/Fe front	30.3	0	0	−2.31	−11.54	0
Rk + 4Re5	Fe zone	30.3–49.3	−1.47	0	0	10.15	−0.54
Rk + 0.5Re7	CH_4 zone	49.3–80.0	−1.41	0	0	1.39	0.54

Note. For each redox species it gives the mass influx/outflux and the production/consumption by the different redox reactions integrated over distance. Positive values refer to influx or production, negative values to outflux or consumption. The decays at the fronts are calculated by applying Equation 34, those at the redox zones by integrating reaction rates between the indicated values of distance (x). The location of the Fe/CH_4 front (49.3 mm) is taken as the location where $r_{Fe} = r_{CH4}$.

Rk + Re3: $CH_2O + O_2 \rightarrow HCO_3^- + H^+$

Re3 − 0.8Re4: $O_2 + 0.4N_2 + 0.4H_2O \rightarrow 0.8NO_3^- + 0.8H^+$

Rk + 0.8Re4: $CH_2O + 0.8NO_3^- \rightarrow HCO_3^- + 0.4N_2 + 0.4H_2O + 0.2H^+$

0.8Re4 − 4Re5: $0.8NO_3^- + 4Fe^{2+} + 9.6H_2O \rightarrow 0.4N_2 + 4Fe(OH)_3(s) + 7.2H^+$

Rk + 4Re5: $CH_2O + 4Fe(OH)_3 + 7H^+ \rightarrow HCO_3^- + 4Fe^{2+} + 10H_2O$

Rk + 0.5Re7: $CH_2O + 0.5H_2O \rightarrow 0.5HCO_3^- + 0.5CH_4 + 0.5H^+$

4.5. Comparison of the PEA With the Fully Kinetic Approach

As discussed in the previous section, a shortcoming of the PEA is that it permits spurious reactions that, although being thermodynamically possible, are not always realistic. This occurs both in our solution and in the numerical model, indicating that it is related to the concept of the PEA and, especially, to the assumption of thermodynamic equilibrium of TEAs. Therefore, in this section we compare the analytical PEA of both the advection and diffusion model with a fully kinetic approach assuming Monod kinetics. We used Phreeqc for the calculation of the latter by incorporating all the TEAs and DOC as new external species without interaction of thermodynamics of the database. We assumed the same spatial and temporal discretization as the models of Sections 4.3 and 4.4. The

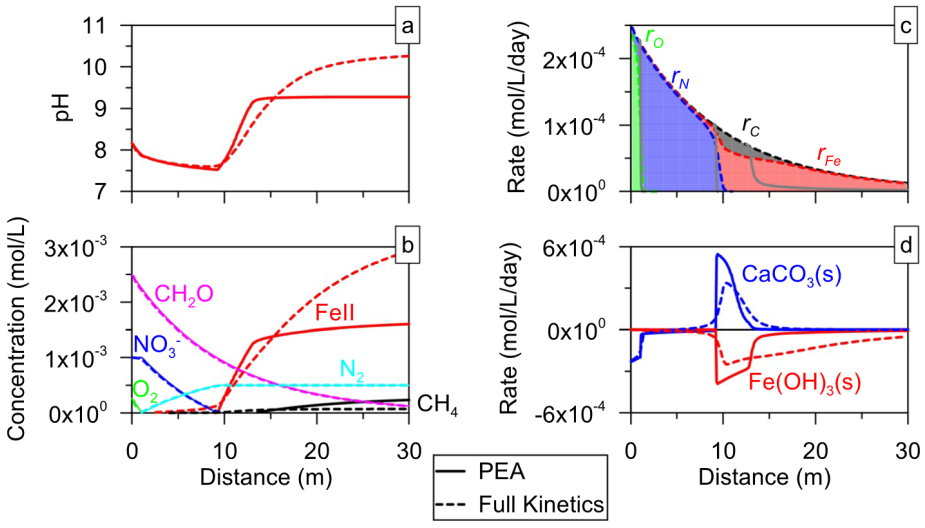

Figure 5. Comparison of the Partial Equilibrium Approach (PEA, continuous lines) with the fully kinetic approach (dashed lines) for the advection model. The gray lines in Figure (c) refer to the PEA results of Figure 3c.

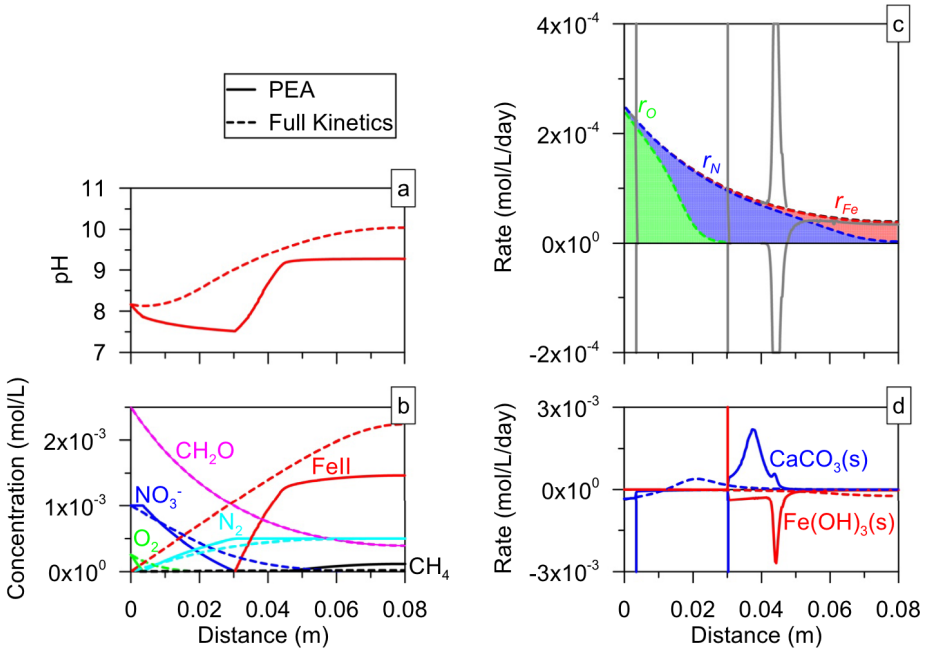

Figure 6. Comparison of the Partial Equilibrium Approach (PEA, continuous lines) with the fully kinetic approach (dashed lines) for the diffusion model. The gray lines in Figure (c) refer to the PEA results of Figure 4c.

model also assumes the four redox reactions of Section 2 to be kinetic. Their rate laws are given by Equations 1–4 with equal λ's. All rate law parameters are shown in Table 1. Although we use a high λ, it is still in the rage of normal values. Values for k_{O2}, $k_{NO_3^-}$, k_{DIC} are similar to those found in the literature. The value for k_{FeII} is more disputable. Concentrations of aqueous Fe(III) are usually very low due to the low solubility of iron oxides. In fact, iron reduction is often assumed not to depend on aqueous Fe(III), which is equivalent to $k_{FeIII} = 0$. We used a value of 1.0×10^{-8} M, which roughly coincides with aqueous Fe(III) concentrations in equilibrium with amorphous $Fe(OH)_3(s)$.

Figures 5 and 6 show the results of the comparison for the advection and diffusion model, respectively. As the fully kinetic approach does not consider the electron (e^-), pe is not shown. For both models, the fully kinetic approach predicts the same concentration of organic carbon and the same total organic carbon oxidation rate ($r_k = r_O + r_N + r_{Fe} + r_C$) as the PEA. This is due to the fact that both approaches use the same Equation 6 for organic carbon oxidation. For the advection model, both approaches show similar results for aerobic oxidation (r_O), denitrification (r_N) and concentrations of O_2, NO_3^-, and N_2. Although the O_2/NO_3^-, and NO_3^-/Fe fronts are smoother for the full kinetic approach, their positions agree with those of the PEA. The main difference between the PEA and the fully kinetic approach is related to the iron reduction and methanogenesis. In general, the fully kinetic approach predicts much less methanogenesis than the PEA. The reason is that only the limit of the Fe(II) stability zone is reached as shown in Figure 1d. Therefore, there will still be enough Fe(III) to inhibit methanogenesis according to Equation 4. As a result, the iron reduction zone is extended and Fe(II) concentrations are larger for the fully kinetic approach.

On the other hand, differences are more important for the diffusion model (Figure 6). The O_2 and NO_3^- penetrate much further when full kinetics are used. Large part of the O_2 diffusing into the domain is used for oxidizing N_2 at the O_2/NO_3^- front when PEA is used (see Table 3). The fully kinetic approach does not admit this and, instead, O_2 is used for oxidizing organic carbon. Neither do the fully kinetics admit formation of NO_3^-. Instead, it diffuses from the inlet, which is evidenced by the gradient of its concentration (Figure 6b). In addition, fully kinetics do not consider NO_3^- formation at the NO_3^-/Fe front. Likewise, as fully kinetics do not allow Fe(II) consumption at the NO_3^-/Fe front, Fe(II) formed by iron reduction can only leave the domain through diffusion, creating clear gradients of Fe(II) concentrations in Figure 6b.

5. Discussion

Our analytical solution was applied and verified with a numerical model code using two very simple one-dimensional steady state cases: one completely advective and the other completely diffusive. Our solution fitted exactly the numerical solution (Figures 3 and 4), showing its adequacy to be implemented. Besides these two tested cases, our solution could be easily extended to 2D and 3D models, transient systems and mixing of various end-members. Extension to 2D and 3D is not trivial, but analytical models has existed for several decades (e.g., Wexler, 1992). Besides analytical models one can also use numerical models for the calculations of the conservative transport (step 1 of the procedure) and of the transport with linear decay (step 2). This is exemplified by Romanov and Dreybrodt (2006) and Guadagnini et al. (2009), who applied numerical models to calculate calcite dissolution albeit without organic carbon oxidation. This implies that there are barely any limits to model flow and conservative transport processes. An interesting application could be organic carbon oxidation in soils requiring the calculation of unsaturated flow, for which hardly any analytical solutions exists. It must be said that in such systems, diffusion of gaseous species (O_2, N_2, and CO_2) can become important processes, which unfortunately cannot be modeled adequately by our semi-analytical solution. Another noteworthy application is organic carbon oxidation in domains with heterogeneous hydraulic conductivity and, consequently, heterogeneous flow and transport. As discussed in a recent review by Carrera et al. (2022) the advection dispersion equation is a poor representation of transport in such domains. This has been acknowledged for conservative transport but is even more relevant for reactive transport and, particularly, for organic carbon oxidation. Zones of low conductivity and low water flow tend to contain water of low redox potential because of the slow influx of TEAs. We conjecture that this can create intricate patterns of redox zones. Analyzing and modeling such patterns by means of traditional numerical reactive transport model codes would be very expensive in CPU time. Our semi-analytical solution, on the other hand, would only require the calculation of conservative transport and transport with linear decay, which is much cheaper. Calculation of gradients and reaction rates can be done straightforwardly in a post-processing fashion. Of course, in low conductivity zones, diffusion can be the main transport mechanism. In such conditions the PEA may produce spurious results as discussed before. On the other hand, an explicit treatment of heterogeneities (i.e., not by dispersion coefficients) would reduce such problems. An analysis of the combined effect of both is beyond the scope of this paper. Anyway, we expect no problems for advective cases with heterogeneous flow but without diffusion and dispersion.

6. Conclusions

In this work, we have developed a semi-analytical solution for organic carbon oxidation coupled to the reduction-oxidation and TEAs sequence assuming the PEA. Like the procedure of De Simoni et al. (2005), it decouples the chemistry from the transport. The chemistry can be calculated using standard speciation codes, such as Phreeqc. In some cases, the chemistry may be simplified by using Heaviside step and Dirac delta functions. Our analytical solution assumes that the sum of the organic carbon oxidation by all TEAs can be simplified by a linear kinetic rate law, which we consider a reasonable assumption, given that we are dealing with an analytical solution. Maybe it can be combined with the analytical solution of Sanchez-Vila et al. (2010) for more kinetic reactions, but this is beyond the scope of the paper.

Our semi-analytical solution was applied and verified with a numerical model code using two very simple one-dimensional steady state cases: one completely advective and the other completely diffusive. Our solution fitted exactly the numerical solution, showing its adequacy to be implemented. In our opinion, another advantage—in comparison with previous analytical solutions—is that any set of equilibrium aqueous complexation and mineral precipitation-dissolution reactions can be incorporated if the minerals are present ubiquitously. For the particular chemical system of our application, this means that we could not incorporate siderite ($FeCO_3$), because it only forms in zones of low redox potential. Another more obvious limitation is that clogging, which is a common phenomenon in organic carbon decay, cannot be handled by our solution, because it affects flow and transport properties. So, in that case, flow and (conservative) transport can no longer be solved independently of the chemistry.

Analytical or semi-analytical solutions do not only benefit from lower CPU times. They can also improve our understanding of the modeled phenomena. Analysis by means of our solution reveals that in diffusive cases assuming the PEA permits substantial N_2 oxidation by O_2, Fe(II) oxidation by NO_3^- and CH_4 oxidation by

$Fe(OH)_3(s)$, taking place near the transition zones between the various TEAs. Reaction rates show spikes (almost Dirac delta functions) at these transition zones, which is difficult to calculate with conventional numerical methods such as finite elements or finite differences, because such methods average rates over cells or elements of finite size. On the other hand, they can be assessed easily with our semi-analytical solution. Most of these reactions are unrealistic in environmental reduction oxidation systems, especially the oxidation of N_2 by O_2. The comparison with the fully kinetic approach showed that, while the use of PEA in purely advective systems does not imply a quantitatively important production of such processes and concentrations are quite similar, in diffusive systems there is an important impact on concentrations and reaction rates. This may be a peculiarity of diffusive systems, but in theory, it may also be relevant for systems with advection and dispersion. Modelers that use the PEA should bear this in mind. At least, this shortcoming of the PEA can now be quantified. For cases with diffusion or dispersion cases, we can calculate rates of spurious reactions and reject the model if these rates are too big in comparison to other terms in the mass balances.

Data Availability Statement

The analytical solution for the advection and diffusion models of Section 4.3 and 4.4 has been coded in an excel file, which is available at [https://doi.org/10.5281/zenodo.6023213]. The code Phreeqc was applied for the chemical batch calculations of Section 4.2 and the numerical models using the PEA (Section 4.3 and 4.4) and fully kinetic approach (Section 4.5). Input files and thermodynamic databases for these models can be downloaded from the same repository.

Acknowledgments
This work was financially supported by MONOPOLIOS (RTI2018-101990-B-100, MINECO/FEDER), MEDISTRAESIII (Pid2019-110212RB-C22, MICINN), as well as the EU project MARADENTRO (PCI2019-103425-WW2017) and the Catalan Research Project RESTORA (ACA210/18/00,040). Additional funding was obtained from the Generalitat de Catalunya (2017 SGR1485). We also would like to thank Carlos Ayora for his constructive comments on the manuscript.

References

Arora, B., Şengör, S. S., Spycher, N. F., & Steefel, C. I. (2015). A reactive transport benchmark on heavy metal cycling in lake sediments. *Computational Geosciences*, *19*, 613–633. https://doi.org/10.1007/s10596-014-9445-8

Barba, C., Folch, A., Gaju, N., Sanchez-Vila, X., Carrasquilla, M., Grau-Martínez, A., & Martínez-Alonso, M. (2019). Microbial community changes induced by managed aquifer recharge activities: Linking hydrogeological and biological processes. *Hydrology and Earth System Sciences*, *23*, 139–154. https://doi.org/10.5194/hess-23-139-2019

Brun, A., & Engesgaard, P. (2002). Modelling of transport and biogeochemical processes in pollution plumes: Literature review and model development. *Journal of Hydrology*, *256*(3–4), 211–227. https://doi.org/10.1016/S0022-1694(01)00547-9

Brun, A., Engesgaard, P., Christensen, T. H., & Rosbjerg, D. (2002). Modelling of transport and biogeochemical processes in pollution plumes: Vejen landfill, Denmark. *Journal of Hydrology*, *256*(3–4), 228–247. https://doi.org/10.1016/S0022-1694(01)00549-2

Canavan, R. W., Van Cappellen, P., Zwolsman, J. J. G., van den Berg, G. A., & Slomp, C. P. (2007). Geochemistry of trace metals in a fresh water sediment: Field results and diagenetic modeling. *The Science of the Total Environment*, *381*(1–3), 263–279. https://doi.org/10.1016/j.scitotenv.2007.04.001

Carrera, J., Saaltink, M. W., Soler-Sagarra, J., Wang, J., & Valhondo, C. (2022). Reactive transport: A review of basic concepts with emphasis on biochemical processes. *Energies*, *15*, 925. https://doi.org/10.3390/en15030925

Christensen, T. H., Bjerg, P. L., Banwart, S. A., Jakobsen, R., Heron, G., & Albrechtsen, H.-J. (2000). Characterization of redox conditions in groundwater contaminant plumes. *Journal of Contaminant Hydrology*, *45*(3), 165–241. https://doi.org/10.1016/S0169-7722(00)00109-1

Chu, M., Kitanidis, P. K., & McCarty, P. L. (2005). Modeling microbial reactions at the plume fringe subject to transverse mixing in porous media: When can the rates of microbial reaction be assumed to be instantaneous? *Water Resourses Research*, *41*, W06002. https://doi.org/10.1029/2004WR003495

Cirpka, O. A., & Valocchi, A. J. (2007). Two-dimensional concentration distribution for mixing-controlled bioreactive transport in steady state. *Advances in Water Resourses*, *30*(6), 1668–1679. https://doi.org/10.1016/j.advwatres.2006.05.022

Cozzarelli, I. M., Suflita, J. M., Ulrich, G. A., Harris, S. H., Scholl, M. A., Schlottmann, J. L., & Christenson, S. (2000). Geochemical and microbiological methods for evaluating anaerobic processes in an aquifer contaminated by landfill leachate. *Environmental Science & Technology*, *34*(18), 4025–4033. https://doi.org/10.1021/es991342b

Curtis, G. P. (2003). Comparison of approaches for simulating reactive solute transport involving organic degradation reactions by multiple terminal electron acceptors. *Computers & Geosciences*, *29*(3), 319–329. https://doi.org/10.1016/S0098-3004(03)00008-6

Dash, S., Borah, S. S., & Kalamdhad, A. S. (2020). Study of the limnology of wetlands through a one-dimensional model for assessing the eutrophication levels induced by various pollution sources. *Ecological Modelling*, *416*, 108907. https://doi.org/10.1016/j.ecolmodel.2019.108907

De Simoni, M., Carrera, J., Sanchez-Vila, X., & Guadagnini, A. (2005). A procedure for the solution of multicomponent reactive transport problems. *Water Resourses Research*, *41*, W11410. https://doi.org/10.1029/2005WR004056

De Simoni, M., Sanchez-Vila, X., Carrera, J., & Saaltink, M. W. (2007). A mixing ratios-based formulation for multicomponent reactive transport. *Water Resourses Research*, *43*, W07419. https://doi.org/10.1029/2006WR005256

Greskowiak, J., Prommer, H., Massmann, G., & Nützmann, G. (2006). Modeling seasonal redox dynamics and the corresponding fate of the pharmaceutical residue phenazone during artificial recharge of groundwater. *Environmental Science & Technology*, *40*(21), 6615–6621. https://doi.org/10.1021/es052506t

Guadagnini, A., Sanchez-Vila, X., Saaltink, M. W., Bussini, M., & Berkowitz, B. (2009). Application of a mixing-ratios based formulation to model mixing-driven dissolution experiments. *Advances in Water Resourses*, *32*, 756–766. https://doi.org/10.1016/j.advwatres.2008.07.005

Hansel, C. M., Lentini, C. J., Tang, Y., Johnston, D. T., Wankel, S. D., & Jardine, P. M. (2015). Dominance of sulfur-fueled iron oxide reduction in low-sulfate freshwater sediments. *The ISME Journal*, *9*(11), 2400–2412. https://doi.org/10.1038/ismej.2015.50

Hunter, K. S., Wang, Y., & Van Cappellen, P. (1998). Kinetic modeling of microbially-driven redox chemistry of subsurface environments: Coupling transport, microbial metabolism and geochemistry. *Journal of Hydrology*, *209*(1), 53–80. https://doi.org/10.1016/S0022-1694(98)00157-7

Jaffé, R., McKnight, D., Maie, N., Cory, R., McDowell, W. H., & Campbell, J. L. (2008). Spatial and temporal variations in DOM composition in ecosystems: The importance of long-term monitoring of optical properties. *Journal of Geophysical Research*, *113*, G04032. https://doi.org/10.1029/2008JG000683

Jakobsen, R. (2007). Redox microniches in groundwater: A model study on the geometric and kinetic conditions required for concomitant Fe oxide reduction, sulfate reduction, and methanogenesis. *Water Resourses Research*, *43*, W12S12. https://doi.org/10.1029/2006WR005663

Jin, Q., & Bethke, C. M. (2003). A new rate law describing microbial respiration. *Applied and Environmental Microbiology*, *69*(4), 2340–2348. https://doi.org/10.1128/AEM.69.4.2340-2348.2003

Lee, P. O., Shoemaker, C., & Olson, J. B. (2019). Wetland soil properties and resident bacterial communities are influenced by changes in elevation. *Wetlands*, *39*(1), 99–112. https://doi.org/10.1007/s13157-018-1077-7

Mayer, K. U., Benner, S. G., Frind, E. O., Thornton, S. F., & Lerner, D. N. (2001). Reactive transport modeling of processes controlling the distribution and natural attenuation of phenolic compounds in a deep sandstone aquifer. *Journal of Contaminant Hydrology*, *53*(3), 341–368. https://doi.org/10.1016/S0169-7722(01)00173-5

Middelburg, J. J. (1989). A simple rate model for organic matter decomposition in marine sediments. *Geochimica et Cosmochimica Acta*, *53*(7), 1577–1581. https://doi.org/10.1016/0016-7037(89)90239-1

Ng, G.-H. C., Rosenfeld, C. E., Santelli, C. M., Yourd, A. R., Lange, J., Duhn, K., & Johnson, N. W. (2020). Microbial and reactive transport modeling evidence for hyporheic flux-driven ryptic sulfur cycling and anaerobic methane oxidation in a sulfate-impacted wetland-stream system. *Journal of Geophysical Research: Biogeosciences*, *125*, e2019JG005185. https://doi.org/10.1029/2019JG005185

Ng, G. H. C., Yourd, A. R., Johnson, N. W., & Myrbo, A. E. (2017). Modeling hydrologic controls on sulfur processes in sulfate-impacted wetland and stream sediments. *Journal of Geophysical Research: Biogeosciences*, *122*, 2435–2457. https://doi.org/10.1002/2017JG003822

Parkhurst, D. L., & Appelo, C. A. J. (1999). *User's guide to PHREEQC (version 2) - A computer program for speciation, reaction-path, 1D-transport, and inverse geochemical calculations* (pp. 99–4259). U.S. Geological Survey.

Postma, D., & Jakobsen, R. (1996). Redox zonation: Equilibrium constraints on the Fe(III)/SO4-reduction interface. *Geochimica et Cosmochimica Acta*, *60*(17), 3169–3175. https://doi.org/10.1016/0016-7037(96)00156-1

Prommer, H., Tuxen, N., & Bjerg, P. L. (2006). Fringe-controlled natural attenuation of phenoxy acids in a landfill plume: Integration of field-scale processes by reactive transport modeling. *Environmental Science & Technology*, *40*(15), 4732–4738. https://doi.org/10.1021/es0603002

Rodríguez-Escales, P., Barba, C., Sanchez-Vila, X., Jacques, D., & Folch, A. (2020). Coupling flow, heat, and reactive transport modeling to reproduce in situ redox potential evolution: Application to an infiltration pond. *Environmental Science & Technology*, *54*(19), 12092–12101. https://doi.org/10.1021/acs.est.0c03056

Rodríguez-Escales, P., Fernàndez-Garcia, D., Drechsel, J., Folch, A., & Sanchez-Vila, X. (2017). Improving degradation of emerging organic compounds by applying chaotic advection in Managed Aquifer Recharge in randomly heterogeneous porous media. *Water Resources Research*, *53*(5), 4376–4392. https://doi.org/10.1002/2016WR020333

Rolle, M., Clement, T. P., Sethi, R., & Di Molfetta, A. (2008). A kinetic approach for simulating redox-controlled fringe and core biodegradation processes in groundwater: Model development and application to a landfill site in Piedmont, Italy. *Hydrological Processes*, *22*(25), 4905–4921. https://doi.org/10.1002/hyp.7113

Romanov, D., & Dreybrodt, W. (2006). Evolution of porosity in the saltwater-freshwater mixing zone of coastal carbonate aquifers: An alternative modelling approach. *Journal of Hydrology*, *329*(3–4), 661–673. https://doi.org/10.1016/j.jhydrol.2006.03.030

Saaltink, M. W., Vilarrasa, V., De Gaspari, F., Silva, O., Carrera, J., & Rötting, T. S. (2013). A method for incorporating equilibrium chemical reactions into multiphase flow models for CO2 storage. *Advances in Water Resources*, *62*, 431–441. https://doi.org/10.1016/j.advwatres.2013.09.013

Sanchez-Vila, X., Donado, L. D., Guadagnini, A., & Carrera, J. (2010). A solution for multicomponent reactive transport under equilibrium and kinetic reactions. *Water Resourses Research*, *46*, W07539. https://doi.org/10.1029/2009WR008439

Schäfer, D., Schäfer, W., & Kinzelbach, W. (1998a). Simulation of reactive processes related to biodegradation in aquifers: 1. Structure of the three-dimensional reactive transport model. *Journal of Contaminant Hydrology*, *31*(1), 167–186. https://doi.org/10.1016/S0169-7722(97)00060-0

Schäfer, D., Schäfer, W., & Kinzelbach, W. (1998b). Simulation of reactive processes related to biodegradation in aquifers: 2. Model application to a column study on organic carbon degradation. *Journal of Contaminant Hydrology*, *31*(1–2), 187–209. https://doi.org/10.1016/S0169-7722(97)00061-2

Stumm, W., & Morgan, J. J. (1996). *Aquatic chemistry, chemical Equilibria and rates in natural waters* (p. 1022). John Wiley & Sons, Inc.

Torrentó, C., Cama, J., Urmentera, J., Otero, N., & Soler, A. (2010). Denitrification of groundwater with pyrite and Thiobacillus denitrificans. *Chemical Geology*, *278*, 80–91. https://doi.org/10.1016/j.chemgeo.2010.09.003

Torres, E., Couture, R. M., Shafei, B., Nardi, A., Ayora, C., & Van Cappellen, P. (2015). Reactive transport modeling of early diagenesis in a reservoir lake affected by acid mine drainage: Trace metals, lake overturn, benthic fluxes and remediation. *Chemical Geology*, *419*, 75–91. https://doi.org/10.1016/j.chemgeo.2015.10.023

Valhondo, C., Carrera, J., Ayora, C., Tubau, I., Martinez-Landa, L., Nödler, K., & Licha, T. (2015). Characterizing redox conditions and monitoring attenuation of selected pharmaceuticals during artificial recharge through a reactive layer. *The Science of the Total Environment*, *512–513*(0), 240–250. https://doi.org/10.1016/j.scitotenv.2015.01.030

van Breukelen, B. M., Griffioen, J., Röling, W. F. M., & vanVerseveld, H. W. (2004). Reactive transport modelling of biogeochemical processes and carbon isotope geochemistry inside a landfill leachate plume. *Journal of Contaminant Hydrology*, *70*(3–4), 249–269. https://doi.org/10.1016/j.jconhyd.2003.09.003

Van Cappellen, P., & Gaillard, J. F. (1996). *Biogeochemical dynamics in aquatic systems*. In P. C. Lichtner, C. I. Steefel, & E. H. Oelkers, (Eds.) *Reactive transport in porous media, Reviews in mineralogy* (Vol. 34, pp. 335–376). Mineralogical Society of America. https://doi.org/10.1515/9781501509797-011

van Genuchten, M. T., & Alves, W. J. (1982). *Analytical solutions of the one-dimensional convective-dispersive solute transport equation*. Technical Bulletin No. 1661 (p. 151). U.S. Department of Agriculture.

Wexler, E. J. (1992). *Analytical solutions for one-, two-, and three-dimensional solute transport in ground-water systems with uniform flow, Techniques of water-Resources Investigations. Book 3, Chapter B7*. U.S. Geological Survey. https://doi.org/10.3133/twri03B7

Zhou, S., Xu, J., Yang, G., & Zhuang, L. (2014). Methanogenesis affected by the co-occurrence of iron(III) oxides and humic substances. *FEMS Microbiology Ecology*, *88*(1), 107–120. https://doi.org/10.1111/1574-6941.12274